Hindawi Publishing Corporation
EURASIP Journal on Wireless Communications and Networking
Volume 2007, Article ID 39871, 9 pages
doi:10.1155/2007/39871

Research Article

Spatial-Temporal Correlation Properties of the 3GPP Spatial Channel Model and the Kronecker MIMO Channel Model

Cheng-Xiang Wang,[1] Xuemin Hong,[1] Hanguang Wu,[2] and Wen Xu[2]

[1] *Joint Research Institute in Signal and Image Processing, School of Engineering and Physical Sciences, Heriot-Watt University, Edinburgh EH14 4AS, UK*
[2] *Baseband Algorithms and Standardization Laboratory, BenQ Mobile, 81667 Munich, Germany*

Received 1 April 2006; Revised 28 November 2006; Accepted 3 December 2006

Recommended by Thushara Abhayapala

The performance of multiple-input multiple-output (MIMO) systems is greatly influenced by the spatial-temporal correlation properties of the underlying MIMO channels. This paper investigates the spatial-temporal correlation characteristics of the spatial channel model (SCM) in the Third Generation Partnership Project (3GPP) and the Kronecker-based stochastic model (KBSM) at three levels, namely, the cluster level, link level, and system level. The KBSM has both the spatial separability and spatial-temporal separability at all the three levels. The spatial-temporal separability is observed for the SCM only at the system level, but not at the cluster and link levels. The SCM shows the spatial separability at the link and system levels, but not at the cluster level since its spatial correlation is related to the joint distribution of the angle of arrival (AoA) and angle of departure (AoD). The KBSM with the Gaussian-shaped power azimuth spectrum (PAS) is found to fit best the 3GPP SCM in terms of the spatial correlations. Despite its simplicity and analytical tractability, the KBSM is restricted to model only the average spatial-temporal behavior of MIMO channels. The SCM provides more insights of the variations of different MIMO channel realizations, but the implementation complexity is relatively high.

1. INTRODUCTION

In the 3rd generation (3G) and beyond-3G (B3G) wireless communication systems, higher data rate transmissions and better quality of services are demanded. This motivates the investigation towards the full exploitation of time, frequency, and more recently, space domains. By deploying spatially separated multiple antenna elements at both ends of the transmission link, multiple-input multiple-output (MIMO) technologies can improve the link reliability and provide a significant increase of the link capacity [1]. It was further shown in [2] that the MIMO channel capacity grows linearly with antenna pairs as long as the environment has sufficiently rich scatterers. To approach the promised theoretical MIMO channel capacity, practical signal processing schemes for MIMO systems have been proposed, for example, space-time processing [3, 4] and space-frequency processing [5].

Both the link capacity and signal processing performance are greatly affected by fading correlation characteristics of the underlying MIMO channels [6]. An appropriate characterization and modeling of MIMO propagation channels are thus indispensable for the development of 3G and B3G systems. In the literature, MIMO channels are often modeled by applying a stochastic approach [7, 8]. Stochastic MIMO channel models can roughly be classified into three types [9], namely, geometrically-based stochastic models (GBSMs), Correlation Based Stochastic Models (CBSMs), and Parametric Stochastic Models (PSMs). A GBSM is derived from a predefined stochastic distribution of scatterers by applying the fundamental laws of reflection, diffraction, and scattering of electromagnetic waves. The well-known GBSMs are one-ring [10], two-ring [11], and elliptical [12] MIMO channel models. CBSMs are another type, in which the spatial correlation properties of a MIMO channel are modeled by statistical means. A Kronecker-based stochastic model (KBSM) [7], which is a simplified CBSM, has been adopted as the core of the link-level MIMO model in the 3rd Generation Partnership Project (3GPP) [13]. The third type is PSMs, which characterize the MIMO channels by using selected parameters such as angle of arrival (AoA) and angle of departure

(AoD). The received signal is modeled as a superposition of waves, and often adopted into a tapped delay-line structure for implementation. Within this category, the widely employed models are the spatial channel model (SCM) [14] for bandwidths up to 5 MHz and the wideband SCM [15] for bandwidths above 5 MHz, specified in the 3GPP.

It is important to mention that the above three types of stochastic MIMO channel models are interrelated. The relationship between a GBSM and a PSM was theoretically analyzed in [16], while the connection between a GBSM and a CBSM was demonstrated in [6]. The mapping between a PSM and a CBSM was addressed only in a few papers [17–19], where the comparison of the spatial-temporal correlation properties of both types of models was not based on the same set of parameters. This leaves us a doubt whether the difference of the spatial-temporal correlation characteristics is caused by the models' structural difference or different parameter generation mechanisms.

The SCM [14] was proposed by the 3GPP for both link- and system-level simulations, while the KBSM [7] was mainly used for the link-level MIMO simulations [13]. Both models have advantages and disadvantages. The SCM can directly generate channel coefficients, while it does not specify the spatial-temporal correlation properties explicitly. It is therefore difficult to connect its simulation results with the theoretical analyses. Also, the implementation complexity of the SCM is high since it has to generate many parameters such as antenna array orientations, mobile directions, delay spread, angular spread (AS), AoDs, AoAs, and phases. On the other hand, a KBSM requires less input parameters and provides elegant and concise analytical expressions for MIMO channel spatial correlation matrices. This makes the KBSM easier to be integrated into a theoretical framework. However, compared with the SCM, KBSMs are often questioned about the oversimplification of MIMO channel characteristics. Although both the SCM and KBSM are well known, some important issues still remain unclear for academia and industry. These issues include the following question (1) what is the major physical phenomenon that makes the fundamental difference of the two models? (2) under what conditions will the two models exhibit similar spatial-temporal correlation characteristics? (3) when will we use the SCM or KBSM as the best tradeoff between the model accuracy and efficiency? The aim of this paper is to find solutions to the above unclear questions. For this purpose, we propose to distinguish the spatial-temporal correlation properties of both models at three levels, namely, the cluster level, link level, and system level. Also, the same parameter generator is used for both models so that the difference of the resulting channel characteristics is caused only by the fundamental structural difference between the SCM and KBSM.

The rest of the paper is organized as follows. Section 2 briefly reviews the 3GPP SCM. Its spatial-temporal correlation characteristics are also analyzed. A KBSM and its spatial-temporal correlation properties are presented in Section 3. Section 4 compares the spatial-temporal correlation properties of the two models. Finally, the conclusions are drawn in Section 5.

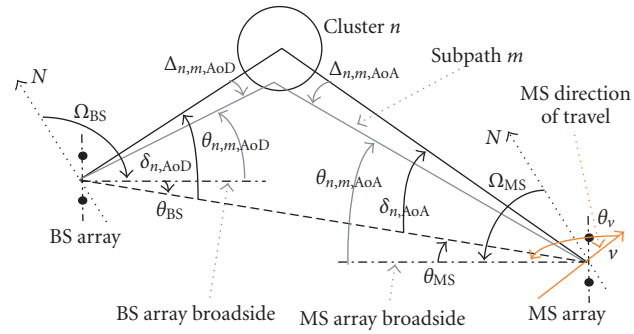

Figure 1: BS and MS angle parameters in the 3GPP SCM with one cluster of scatterers [14].

2. THE 3GPP SCM AND ITS SPATIAL-TEMPORAL CORRELATION CHARACTERISTICS

In this paper, we will consider a downlink system where a base station (BS) transmits to a mobile station (MS). The developed results and conclusions, however, can be applied to uplink systems as well.

2.1. Angle parameters and the concept of three levels

The 3GPP SCM [14] emulates the double-directional and clustering effects of small scale fading mechanisms in a variety of environments, such as suburban macrocell, urban macrocell, and urban microcell. It considers N clusters of scatterers. A cluster can be considered as a resolvable path. Within a resolvable path (cluster), there are M subpaths which are regarded as the unresolvable rays. A simplified plot of the SCM is given in Figure 1 [14], where only one cluster of scatterers is shown as an example. Here, θ_v is the angle of the MS velocity vector with respect to the MS broadside, $\theta_{n,m,\mathrm{AoD}}$ is the absolute AoD for the mth ($m = 1,\ldots,M$) subpath of the nth ($n = 1,\ldots,N$) path at the BS with respect to the BS broadside, and $\theta_{n,m,\mathrm{AoA}}$ is the absolute AoA for the mth subpath of the nth path at the MS with respect to the MS broadside. The absolute AoD $\theta_{n,m,\mathrm{AoD}}$ and absolute AoA $\theta_{n,m,\mathrm{AoA}}$ are given by (see [14])

$$\begin{aligned}\theta_{n,m,\mathrm{AoD}} &= \theta_{\mathrm{BS}} + \delta_{n,\mathrm{AoD}} + \Delta_{n,m,\mathrm{AoD}} \\ &= \theta_{n,\mathrm{AoD}} + \Delta_{n,m,\mathrm{AoD}},\end{aligned} \tag{1}$$

$$\begin{aligned}\theta_{n,m,\mathrm{AoA}} &= \theta_{\mathrm{MS}} + \delta_{n,\mathrm{AoA}} + \Delta_{n,m,\mathrm{AoA}} \\ &= \theta_{n,\mathrm{AoA}} + \Delta_{n,m,\mathrm{AoA}},\end{aligned} \tag{2}$$

respectively, where θ_{BS} is the line-of-sight (LOS) AoD direction between the BS and MS with respect to the broadside of the BS array, θ_{MS} is the angle between the BS-MS LOS and the MS broadside, $\delta_{n,\mathrm{AoD}}$ and $\delta_{n,\mathrm{AoA}}$ are the AoD and AoA for the nth path with respect to the LOS AoD and the LOS AoA, respectively, $\Delta_{n,m,\mathrm{AoD}}$ and $\Delta_{n,m,\mathrm{AoA}}$ are the offsets for the mth subpath of the nth path with respect to $\delta_{n,\mathrm{AoD}}$ and $\delta_{n,\mathrm{AoA}}$, respectively, $\theta_{n,\mathrm{AoD}} = \theta_{\mathrm{BS}} + \delta_{n,\mathrm{AoD}}$ and $\theta_{n,\mathrm{AoA}} = \theta_{\mathrm{MS}} + \delta_{n,\mathrm{AoA}}$ are called the mean AoD and mean AoA, respectively.

Table 1: 3GPP SCM subpath AoD and AoA offsets.

Subpath number (m)	Offset for a 2 deg AS at BS (Macrocell) $\Delta_{n,m,\text{AoD}}$ (degrees)	Offset for a 5 deg AS at BS (Microcell) $\Delta_{n,m,\text{AoD}}$ (degrees)	Offset for a 35 deg AS at MS $\Delta_{n,m,\text{AoA}}$ (degrees)
1, 2	±0.0894	±0.2236	±1.5649
3, 4	±0.2826	±0.7064	±4.9447
5, 6	±0.4984	±1.2461	±8.7224
7, 8	±0.7431	±1.8578	±13.0045
9, 10	±1.0257	±2.5642	±17.9492
11, 12	±1.3594	±3.3986	±23.7899
13, 14	±1.7688	±4.4220	±30.9538
15, 16	±2.2961	±5.7403	±40.1824
17, 18	±3.0389	±7.5974	±53.1816
19, 20	±4.3101	±10.7753	±75.4274

From (1) and (2), it is clear that the absolute AoD/AoA is determined by three parameters, each of which can be either a constant or a random variable. Different reasonable combinations (constant or random variable) of those three parameters correspond to different channel behaviors with different physical implications. Based on the hierarchy of the construction of $\theta_{n,m,\text{AoD}}/\theta_{n,m,\text{AoA}}$, we propose to distinguish the model properties at three levels, that is, the cluster level, link level, and system level.

At the *cluster* level, we assume that the cell layout, user locations, antenna orientations, and cluster positions all remain unchanged, only the scatterer positions within a *cluster* may vary based on a given distribution. This implies that the mean AoD $\theta_{n,\text{AoD}} = \theta_{\text{BS}} + \delta_{n,\text{AoD}}$ and mean AoA $\theta_{n,\text{AoA}} = \theta_{\text{MS}} + \delta_{n,\text{AoA}}$ are kept constant, while the subpath AoD offsets $\Delta_{n,m,\text{AoD}}$ and subpath AoA offsets $\Delta_{n,m,\text{AoA}}$ are determined by the distribution of scatterers within a cluster, that is, the subpath power azimuth spectrum (PAS). Clearly, cluster-level characteristics are only related to subpath PASs within clusters. Note that for the SCM, specified constant values are given for $\Delta_{n,m,\text{AoD}}$ and $\Delta_{n,m,\text{AoA}}$ (see [14, Table 5.2]) to emulate the subpath statistics in various environments. For the readers' convenience, they are repeated in Table 1.

At the *link* level, the cell layout, user locations, and antenna orientations are still kept constant, which indicates that we only consider *one link* consisting of a single BS and a single MS. It follows that θ_{BS} and θ_{MS} are fixed. The cluster positions may change following a distribution, that is, $\delta_{n,\text{AoD}}$ and $\delta_{n,\text{AoA}}$ are random variables. Note that link-level properties are obtained by taking the average of the corresponding cluster-level characteristics over all the realizations of $\delta_{n,\text{AoD}}$ and $\delta_{n,\text{AoA}}$.

At the *system* level, θ_{BS}, θ_{MS}, $\delta_{n,\text{AoD}}$, and $\delta_{n,\text{AoD}}$ are all considered as random variables. It is important to mention that the actual values of θ_{BS} and θ_{MS} depend on the relative MS-BS positions, which are determined according to the cell layout and the broadside of the instant antenna array orientations. Since both θ_{BS} and θ_{MS} are random variables, we actually consider multiple cells BSs and MSs as a complete *system*. Similarly, the system level properties are obtained by averaging all realizations of θ_{BS} and θ_{MS} based on the link-level statistics. For clarity, we show in Table 2 the choices of θ_{BS}, θ_{MS}, $\delta_{n,\text{AoD}}$, $\delta_{n,\text{AoD}}$, $\Delta_{n,m,\text{AoD}}$, and $\Delta_{n,m,\text{AoA}}$ as either constants or random variables at three levels.

Table 2: The angle parameters of the SCM at three levels.

	$\Delta_{n,m,\text{AoD}}$ $\Delta_{n,m,\text{AoA}}$	$\delta_{n,\text{AoD}}$ $\delta_{n,\text{AoA}}$	θ_{BS} θ_{MS}
Cluster level	Constant	Constant	Constant
Link level	Constant	Random	Constant
System level	Constant	Random	Random

To understand better the relationship of the above defined three levels, let us now consider an example of a multi-user cellular system with multiple cells BSs, and MSs. This system consists of multiple single-user links, where each link relates to the connection of a single BS and a single MS. Suppose that each link is corresponding to a wideband channel model adopting the tapped-delay-line structure. Then, each cluster is in fact associated with a single tap with a given delay. Clearly, a lower-level channel behavior reflects only a snapshot (or a realization/simulation run) of the higher-level channel behavior.

2.2. Spatial-temporal correlation properties

For an S element linear BS array and a U element linear MS array, the channel coefficients for one of the N paths are given by a U—by—S matrix of complex amplitudes. By denoting the channel matrix for the nth path ($n = 1, \ldots, N$) as $\mathbf{H}_n(t)$, we can express the (u, s)th ($s = 1, \ldots, S$ and $u = 1, \ldots, U$) component of $\mathbf{H}_n(t)$ as follows:

$$h_{u,s,n}(t) = \sqrt{\frac{P_n}{M}} \sum_{m=1}^{M} \exp\left[jkd_s \sin\left(\theta_{n,m,\text{AoD}}\right)\right] \cdot \exp\left[jkd_u \sin\left(\theta_{n,m,\text{AoA}}\right)\right] \exp\left(j\Phi_{n,m}\right) \cdot \exp\left[jk\|\mathbf{v}\| \cos\left(\theta_{n,m,\text{AoA}} - \theta_v\right)t\right], \tag{3}$$

where $j = \sqrt{-1}$, k is the wave number $2\pi/\lambda$ with λ denoting the carrier wavelength in meters, P_n is the power of the nth path, d_s is the distance in meters from BS antenna element s

to the reference ($s = 1$) antenna, d_u is the distance in meters from MS antenna element u to the reference ($u = 1$) antenna, $\Phi_{n,m}$ is the phase of the mth subpath of the nth path, and $\|\mathbf{v}\|$ is the magnitude of the MS velocity vector. It is important to mention that (3) is a simplified version of the expression $h_{u,s,n}(t)$ in [14] by neglecting the shadowing factor σ_{SF} and assuming that the antenna gains of each array element $G_{\mathrm{BS}}(\theta_{n,m,\mathrm{AoD}}) = G_{\mathrm{MS}}(\theta_{n,m,\mathrm{AoA}}) = 1$.

The normalized complex spatial-temporal correlation function between two arbitrary channel coefficients connecting two different sets of antenna elements is defined as

$$\rho_{s_2u_2}^{s_1u_1}(\Delta d_s, \Delta d_u, \tau) = E\left\{\frac{h_{u_1,s_1,n}(t)h_{u_2,s_2,n}^*(t+\tau)}{\sigma_{h_{u_1,s_1,n}}\sigma_{h_{u_2,s_2,n}}}\right\}, \tag{4}$$

where $E\{\cdot\}$ denotes the statistical average, $\sigma_{h_{u_1,s_1,n}} = \sqrt{P_n}$ and $\sigma_{h_{u_2,s_2,n}} = \sqrt{P_n}$ are the standard deviations of $h_{u_1,s_1,n}(t)$ and $h_{u_2,s_2,n}(t)$, respectively. The substitution of (3) into (4) results in

$$\begin{aligned}\rho_{s_2u_2}^{s_1u_1}(\Delta d_s, \Delta d_u, \tau) &= \frac{1}{M}\sum_{m=1}^{M} E\{\exp[jk\Delta d_s \sin(\theta_{n,m,\mathrm{AoD}})] \\ &\quad \cdot \exp[-jk\|\mathbf{v}\|\cos(\theta_{n,m,\mathrm{AoA}} - \theta_v)\tau] \\ &\quad \cdot \exp[jk\Delta d_u \sin(\theta_{n,m,\mathrm{AoA}})]\},\end{aligned} \tag{5}$$

where $\Delta d_s = |d_{s_1} - d_{s_2}|$ and $\Delta d_u = |d_{u_1} - d_{u_2}|$ denote the relative BS and MS antenna element spacings, respectively. Note that $E\{\exp(\Phi_{n,m_1} - \Phi_{n,m_2})\} = 0$ when $m_1 \neq m_2$ was used in the derivation of (5). From (5), the spatial cross-correlation function (CCF) and temporal autocorrelation function (ACF) can also be obtained.

2.2.1. Spatial CCFs

By imposing $\tau = 0$ in (5), we get the spatial CCF $\rho_{s_2u_2}^{s_1u_1}(\Delta d_s, \Delta d_u)$ between two arbitrary channel coefficients at the same time instant:

$$\begin{aligned}\rho_{s_2u_2}^{s_1u_1}(\Delta d_s, \Delta d_u) &= \frac{1}{M}\sum_{m=1}^{M} E\{\exp[jk\Delta d_s \sin(\theta_{n,m,\mathrm{AoD}})] \\ &\quad \cdot \exp[jk\Delta d_u \sin(\theta_{n,m,\mathrm{AoA}})]\}.\end{aligned} \tag{6}$$

Some special cases of (6) can be observed as follows.

(i) $\Delta d_s = 0$: this results in the spatial CCF observed at the MS

$$\rho_{u_1u_2}^{\mathrm{MS}}(\Delta d_u) = \frac{1}{M}\sum_{m=1}^{M} E\{\exp[jk\Delta d_u \sin(\theta_{n,m,\mathrm{AoA}})]\}. \tag{7}$$

(ii) $\Delta d_u = 0$: the resulting spatial CCF observed at the BS is

$$\rho_{s_1s_2}^{\mathrm{BS}}(\Delta d_s) = \frac{1}{M}\sum_{m=1}^{M} E\{\exp[jk\Delta d_s \sin(\theta_{n,m,\mathrm{AoD}})]\}. \tag{8}$$

It is important to mention that (6), (7), and (8) are valid expressions for the spatial CCFs of the SCM at all the three levels. However, at the cluster level, $E\{\cdot\}$ can be omitted since all the involved angle parameters are kept constant. Note that the spatial CCF in (6) cannot simply be broken down into the multiplication of a receive term (7) and a transmit term (8). This indicates that the spatial CCF of the 3GPP SCM is in general not separable.

(iii) $M \to \infty$: from (6), we have

$$\begin{aligned}&\lim_{M\to\infty}\rho_{s_2u_2}^{s_1u_1}(\Delta d_s, \Delta d_u) \\ &\quad = \int_0^{2\pi}\int_0^{2\pi} p_{us}(\phi_{n,\mathrm{AoD}}, \phi_{n,\mathrm{AoA}})\exp[jk\Delta d_u \sin(\phi_{n,\mathrm{AoA}})] \\ &\qquad \cdot \exp[jk\Delta d_s \sin(\phi_{n,\mathrm{AoD}})]\, d\phi_{n,\mathrm{AoD}}\, d\phi_{n,\mathrm{AoA}},\end{aligned} \tag{9}$$

where $p_{us}(\phi_{n,\mathrm{AoD}}, \phi_{n,\mathrm{AoA}})$ represents the joint probability density function (PDF) of the AoD and AoA.

(iv) $\Delta d_s = 0$ and $M \to \infty$: from (7), we have

$$\begin{aligned}&\lim_{M\to\infty}\rho_{u_1u_2}^{\mathrm{MS}}(\Delta d_u) \\ &\quad = \int_0^{2\pi}\exp[jk\Delta d_u \sin(\phi_{n,\mathrm{AoA}})]\, p_u(\phi_{n,\mathrm{AoA}})\, d\phi_{n,\mathrm{AoA}},\end{aligned} \tag{10}$$

where $p_u(\phi_{n,\mathrm{AoA}})$ stands for the PDF of the AoA.

(v) $\Delta d_u = 0$ and $M \to \infty$: from (8), we have

$$\begin{aligned}&\lim_{M\to\infty}\rho_{s_1,s_2}^{\mathrm{BS}}(\Delta d_s) \\ &\quad = \int_0^{2\pi}\exp[jk\Delta d_s \sin(\phi_{n,\mathrm{AoD}})]\, p_s(\phi_{n,\mathrm{AoD}})\, d\phi_{n,\mathrm{AoD}},\end{aligned} \tag{11}$$

where $p_s(\phi_{n,\mathrm{AoD}})$ denotes the PDF of the AoD.

2.2.2. The temporal ACF

Let $\Delta d_s = 0$ and $\Delta d_u = 0$ in (5), we obtain the temporal ACF:

$$\begin{aligned}r(\tau) &= \frac{1}{M}\sum_{m=1}^{M} E\{\exp[-jk\|\mathbf{v}\|\cos(\theta_{n,m,\mathrm{AoA}} - \theta_v)\tau]\} \\ &= \rho_{s_2u_2}^{s_1u_1}(0, 0, \tau).\end{aligned} \tag{12}$$

Again, the above expression is valid for the SCM at all the three levels. The comparison of (5), (6), and (12) clearly tells us that the spatial-temporal correlation function $\rho_{s_2u_2}^{s_1u_1}(\Delta d_s, \Delta d_u, \tau)$ is not simply the product of the spatial CCF $\rho_{s_2u_2}^{s_1u_1}(\Delta d_s, \Delta d_u)$ and the temporal ACF $r(\tau)$. Therefore, the spatial-temporal correlation of the SCM is in general not separable as well.

3. THE KBSM AND ITS SPATIAL-TEMPORAL CORRELATION CHARACTERISTICS

The KBSM assumes that the transmission coefficients of a narrowband MIMO channel are complex Gaussian distributed with identical average powers [7]. The channel can

therefore be fully characterized by its first- and second-order statistics. It is further assumed that all the antenna elements in the two arrays have the same polarization and radiation pattern [7].

3.1. Spatial CCFs

Let us still consider a downlink transmission system with an S element linear BS array and a U element linear MS array. The complex spatial CCF at the MS is given by (see [20])

$$\hat{\rho}^{\mathrm{MS}}_{u_1u_2}(\Delta d_u) = \int_0^{2\pi} \exp\left[jk\Delta d_u \sin\left(\hat{\theta}_{\mathrm{AoA}}\right)\right] p_u\left(\hat{\theta}_{\mathrm{AoA}}\right) d\hat{\theta}_{\mathrm{AoA}}. \tag{13}$$

In (13), $p_u(\hat{\theta}_{\mathrm{AoA}})$ denotes the PAS related to the absolute AoA $\hat{\theta}_{\mathrm{AoA}}$. In the literature, different functions have been proposed for the PAS, such as a cosine raised function [21], a Gaussian function [22], a uniform function [23], and a Laplacian function [24]. Note that the PAS here has been normalized in such a way that $\int_0^{2\pi} p_u(\hat{\theta}_{\mathrm{AoA}})d\hat{\theta}_{\mathrm{AoA}} = 1$ is fulfilled. Therefore, $p_u(\hat{\theta}_{\mathrm{AoA}})$ is actually identical with the PDF of the AoA $\hat{\theta}_{\mathrm{AoA}}$. Analogous to the AoA $\theta_{n,m,\mathrm{AoA}}$ for the SCM in (2), $\hat{\theta}_{\mathrm{AoA}}$ can also be written as $\hat{\theta}_{\mathrm{AoA}} = \hat{\theta}_{\mathrm{MS}} + \hat{\delta}_{\mathrm{AoA}} + \Delta\hat{\theta}_{\mathrm{AoA}} = \hat{\theta}_{0,\mathrm{AoA}} + \Delta\hat{\theta}_{\mathrm{AoA}}$, where $\hat{\theta}_{\mathrm{MS}}$, $\hat{\delta}_{\mathrm{AoA}}$, $\Delta\hat{\theta}_{\mathrm{AoA}}$, and $\hat{\theta}_{0,\mathrm{AoA}}$ have similar meanings to θ_{MS}, $\delta_{n,\mathrm{AoA}}$, $\Delta_{n,m,\mathrm{AoA}}$, and $\theta_{n,\mathrm{AoA}}$, respectively.

The spatial CCF at the BS between antenna elements s_1 and s_2 can be expressed as (see [20])

$$\hat{\rho}^{\mathrm{BS}}_{s_1s_2}(\Delta d_s) = \int_0^{2\pi} \exp\left[jk\Delta d_s \sin\left(\hat{\theta}_{\mathrm{AoD}}\right)\right] p_s\left(\hat{\theta}_{\mathrm{AoD}}\right) d\hat{\theta}_{\mathrm{AoD}}, \tag{14}$$

where $p_s(\hat{\theta}_{\mathrm{AoD}})$ is the PAS related to the absolute AoD. Due to the normalization, $p_s(\hat{\theta}_{\mathrm{AoD}})$ is also regarded as the PDF of the AoD. Similar to the AoD for the SCM in (1), the equality $\hat{\theta}_{\mathrm{AoD}} = \hat{\theta}_{\mathrm{BS}} + \hat{\delta}_{\mathrm{AoD}} + \Delta\hat{\theta}_{\mathrm{AoD}} = \hat{\theta}_{0,\mathrm{AoD}} + \Delta\hat{\theta}_{\mathrm{AoD}}$ is fulfilled, where $\hat{\theta}_{\mathrm{BS}}$, $\hat{\delta}_{\mathrm{AoD}}$, $\Delta\hat{\theta}_{\mathrm{AoD}}$, and $\hat{\theta}_{0,\mathrm{AoD}}$ have similar definitions to θ_{BS}, $\delta_{n,\mathrm{AoD}}$, $\Delta_{n,m,\mathrm{AoD}}$, and $\theta_{n,\mathrm{AoD}}$, respectively.

The KBSM further assumes that $\hat{\rho}^{\mathrm{BS}}_{s_1s_2}(\Delta d_s)$ and $\hat{\rho}^{\mathrm{MS}}_{u_1u_2}(\Delta d_u)$ are independent of u and s, respectively. This implies that the spatial CCF $\hat{\rho}^{s_1u_1}_{s_2u_2}(\Delta d_s, \Delta d_u)$ between two arbitrary transmission coefficients has the separability property and is simply the product of $\hat{\rho}^{\mathrm{BS}}_{s_1s_2}(\Delta d_s)$ and $\hat{\rho}^{\mathrm{MS}}_{u_1u_2}(\Delta d_u)$, that is,

$$\hat{\rho}^{s_1u_1}_{s_2u_2}(\Delta d_s, \Delta d_u) = \hat{\rho}^{\mathrm{BS}}_{s_1s_2}(\Delta d_s)\hat{\rho}^{\mathrm{MS}}_{u_1u_2}(\Delta d_u). \tag{15}$$

Thus, the spatial correlation matrix $\hat{\mathbf{R}}_{\mathrm{MIMO}}$ of the MIMO channel can be written as the Kronecker product of $\hat{\mathbf{R}}_{\mathrm{BS}}$ and $\hat{\mathbf{R}}_{\mathrm{MS}}$ [7], that is, $\hat{\mathbf{R}}_{\mathrm{MIMO}} = \hat{\mathbf{R}}_{\mathrm{BS}} \otimes \hat{\mathbf{R}}_{\mathrm{MS}}$, where $\otimes$ represents the Kronecker product, $\hat{\mathbf{R}}_{\mathrm{BS}}$ and $\hat{\mathbf{R}}_{\mathrm{MS}}$ are the spatial correlation matrices at the BS and MS, respectively.

3.2. The temporal ACF

The temporal ACF of the KBSM is determined by the inverse Fourier transform of the Doppler power spectrum density (PSD). When the Doppler PSD is of the U-shape [25], the temporal ACF is given by the well-known Bessel function, that is, $\hat{r}(\tau) = J_0(2\pi\|\nu\|\tau/\lambda)$.

Besides the spatial separability, the above construction of the KBSM also demonstrates the spatial-temporal separability. This allows us to express the spatial-temporal correlation function $\hat{\rho}^{s_1u_1}_{s_2u_2}(\Delta d_s, \Delta d_u, \tau)$ of the KBSM as the product of the individual spatial and temporal correlations, that is,

$$\hat{\rho}^{s_1u_1}_{s_2u_2}(\Delta d_s, \Delta d_u, \tau) = \hat{\rho}^{s_1u_1}_{s_2u_2}(\Delta d_s, \Delta d_u)\hat{r}(\tau). \tag{16}$$

4. COMPARISONS BETWEEN THE SCM AND KBSM

4.1. Spatial CCFs

The comparison of (6) and (15) clearly shows the fundamental difference between the SCM and KBSM. The SCM assumes a finite number of subpaths in each path, while the KBSM simply assumes a very large or even infinite number of multipath components. The AoD and AoA are assumed to be independently distributed in the KBSM, while correlated in the SCM. This is also the reason why the spatial CCF is always separable for the KBSM but not always for the SCM. On the other hand, the comparison of (10) and (13) as well as the comparison of (11) and (14) tells us that both models tend to have the equivalent spatial CCFs under all of the following three conditions: (1) the number M of subpaths in each path for the SCM tends to infinity. (2) Two links share the same antenna element at one end, that is, $\Delta d_s = 0$ or $\Delta d_u = 0$. This corresponds to the spatial CCFs at either the MS or the BS. (3) The same set of angle parameters is used for both models.

The subpath AoA and AoD offsets are fixed values (see Table 1) for the SCM, but are described by PDFs for the KBSM. Our first task is to find out which candidates [22–24] should be employed for the PDFs of the subpath AoD offset $\Delta\hat{\theta}_{\mathrm{AoD}}$ and subpath AoA offset $\Delta\hat{\theta}_{\mathrm{AoA}}$ in the KBSM in order to fit well its spatial CCFs to those of the SCM with the given set of parameters. For this purpose, we keep the mean AoD ($\theta_{n,\mathrm{AoD}}, \hat{\theta}_{0,\mathrm{AoD}}$) and mean AoA ($\theta_{n,\mathrm{AoA}}, \hat{\theta}_{0,\mathrm{AoA}}$) constant and the same for both models. Without loss of generality, $\theta_{n,\mathrm{AoD}} = \hat{\theta}_{0,\mathrm{AoD}} = 60^\circ$ and $\theta_{n,\mathrm{AoA}} = \hat{\theta}_{0,\mathrm{AoA}} = 60^\circ$ were chosen. In this case, we actually consider the cluster-level spatial CCFs for both models. As discussed earlier, the best fit subpath PASs for the KBSM should give the smallest difference between $\lim_{M\to\infty}\rho^{\mathrm{MS}}_{u_1u_2}(\Delta d_u)$ in (10) and $\hat{\rho}^{\mathrm{MS}}_{u_1u_2}(\Delta d_s)$ in (13), as well as $\lim_{M\to\infty}\rho^{\mathrm{BS}}_{s_1s_2}(\Delta d_s)$ in (11) and $\hat{\rho}^{\mathrm{BS}}_{s_1s_2}(\Delta d_s)$ in (14). To approximate the assumption of $M \to \infty$ in the SCM, we used the three sets of subpath AoA/AoD offsets given in Table 1 and interpolated them 100 times, resulting in the so-called interpolated SCM. Figure 2 plots the absolute values of the resulting spatial CCFs at the BS (AS = 2° for macrocell and AS = 5° for microcell) and MS (AS = 35°) as functions of the normalized antenna spacings $\Delta d_s/\lambda$ and $\Delta d_u/\lambda$, respectively, for both the SCM and interpolated SCM. In this figure, we also include the corresponding absolute values of the spatial CCFs for the KBSM with uniform, truncated Gaussian, and truncated Laplacian subpath PASs. Note that the method of

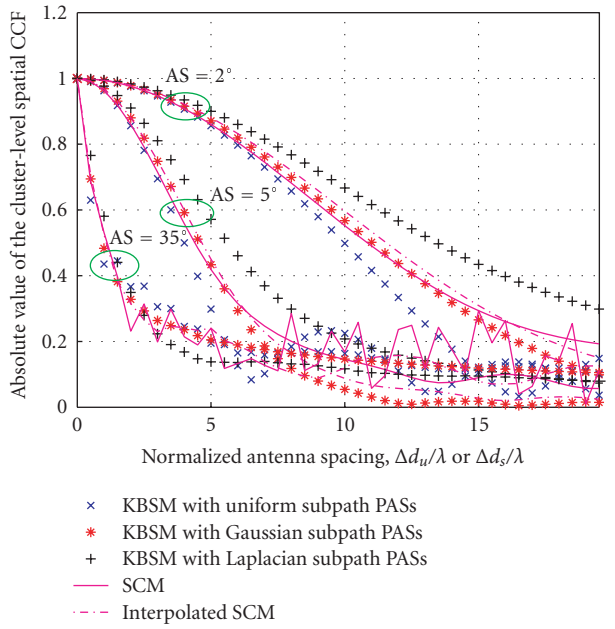

FIGURE 2: The absolute values of the cluster-level spatial CCFs of the SCM, interpolated SCM, and KBSMs with uniform, Gaussian, and Laplacian subpath PASs (mean AoA/AoD = 60°).

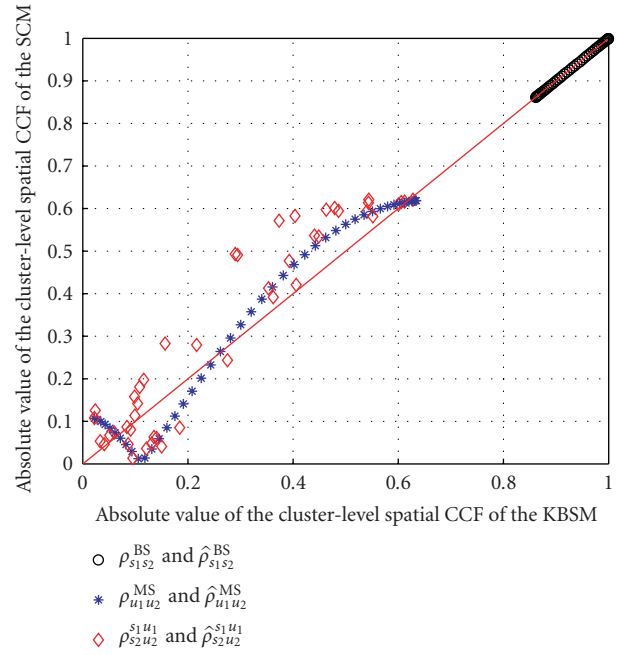

FIGURE 3: The absolute values of the cluster-level spatial CCFs of the SCM and KBSM with Gaussian subpath PASs ($\Delta d_s/\lambda = 1$, $\Delta d_u/\lambda = 1$, BS AS = 5°, MS AS = 35°).

Bessel series expansion [20] was applied here to calculate (13) and (14) for the KBSM. From Figure 2, the following observations can be obtained: (1) the KBSM with the truncated Gaussian subpath PASs provides the best fitting to both the SCM and interpolated SCM. This is interesting by considering the fact that the 3GPP actually suggested a Laplacian distribution for the AoD PAS and either a Laplacian or a uniform distribution for the AoA PAS in its link-level calibration [14]. However, this observation conforms to the measurement result in [26], where a Gaussian PDF was found to best match the measured azimuth PDF. (2) A larger AS results in smaller spatial correlations. The same conclusion was also mentioned in [7]. (3) The spatial CCFs at the BS, that is, AS = 2° and 5°, of the SCM can match well the corresponding ideal values, approximated here by those of the interpolated SCM. However, the spatial CCF at the MS, that is, AS = 35°, of the SCM fluctuates unstably around that of the interpolated SCM. This is caused by the so-called "implementation loss" due to the insufficient number M of subpaths used in the SCM. It is therefore suggested that in the 3GPP SCM, the employed number of subpaths $M = 20$ is not sufficient and should be increased in order to improve its simulation accuracy of the cluster level spatial CCF at the MS. In the following, using the same parameter generating procedure [14, 27], we will compare the spatial CCFs $\rho_{s_2u_2}^{s_1u_1}(\Delta d_s, \Delta d_u)$ in (6), $\rho_{u_1u_2}^{\mathrm{MS}}(\Delta d_u)$ in (7), and $\rho_{s_1s_2}^{\mathrm{BS}}(\Delta d_s)$ in (8) of the SCM with $\hat{\rho}_{s_2u_2}^{s_1u_1}(\Delta d_s, \Delta d_u)$ in (15), $\hat{\rho}_{u_1u_2}^{\mathrm{MS}}(\Delta d_u)$ in (13), and $\hat{\rho}_{s_1s_2}^{\mathrm{BS}}(\Delta d_s)$ in (14) of the KBSM having Gaussian subpath PASs at the three levels. The normalized BS antenna spacing $\Delta d_s/\lambda = 1$ was chosen to calculate (6), (8), (14), and (15), while the normalized MS antenna spacing $\Delta d_u/\lambda = 1$ was selected for computing (6), (7), (13), and (15). The subpath angle offsets $\Delta_{n,m,\mathrm{AoD}}$ and $\Delta_{n,m,\mathrm{AoA}}$ of the SCM were taken from Table 1 with AS = 5° and AS = 35°, respectively.

Figure 3 compares the absolute values of the cluster-level spatial CCFs of the SCM and KBSM. Forty constant values were taken from [0, 90°) for both the mean AoD ($\theta_{n,\mathrm{AoD}}$, $\hat{\theta}_{0,\mathrm{AoD}}$) and mean AoA ($\theta_{n,\mathrm{AoA}}$, $\hat{\theta}_{0,\mathrm{AoA}}$). From this figure, it is obvious that $\rho_{s_1s_2}^{\mathrm{BS}}(\Delta d_s) \approx \hat{\rho}_{s_1s_2}^{\mathrm{BS}}(\Delta d_s)$ holds since all the values are located in the diagonal line. The relatively small difference between $\rho_{u_1u_2}^{\mathrm{MS}}(\Delta d_u)$ and $\hat{\rho}_{u_1u_2}^{\mathrm{MS}}(\Delta d_u)$ comes mostly from the above-mentioned "implementation loss." On the other hand, $\rho_{s_2u_2}^{s_1u_1}(\Delta d_s, \Delta d_u)$ differs significantly from $\hat{\rho}_{s_2u_2}^{s_1u_1}(\Delta d_s, \Delta d_u)$. This clearly tells us that the fundamental difference exists between the SCM and KBSM at the cluster level since the spatial separability is not fulfilled for the SCM. Figure 4 illustrates the absolute values of the link level spatial CCFs versus the normalized MS antenna spacing $\Delta d_u/\lambda$ for both the SCM and KBSM. Here, $\theta_{\mathrm{BS}} = 50°$, $\theta_{\mathrm{MS}} = 195°$, $\delta_{n,\mathrm{AoD}} = \hat{\delta}_{\mathrm{AoD}}$ are considered as uniformly distributed random variables located in the interval $[-40°, 40°)$, while $\delta_{n,\mathrm{AoA}} = \hat{\delta}_{\mathrm{AoA}}$ are Gaussian distributed random variables [14]. To calculate the average in (6) and (7), 1000 random realizations of the cluster position parameters $\delta_{n,\mathrm{AoD}}$ and $\delta_{n,\mathrm{AoA}}$ were used. Clearly, good agreements are found in terms of the link-level spatial CCFs between the SCM and KBSM. It follows that the SCM has the same property of the spatial separability as the KBSM at the link-level. In Figure 5, we demonstrate the absolute values of the system level spatial CCFs versus the normalized MS antenna spacing $\Delta d_u/\lambda$ for

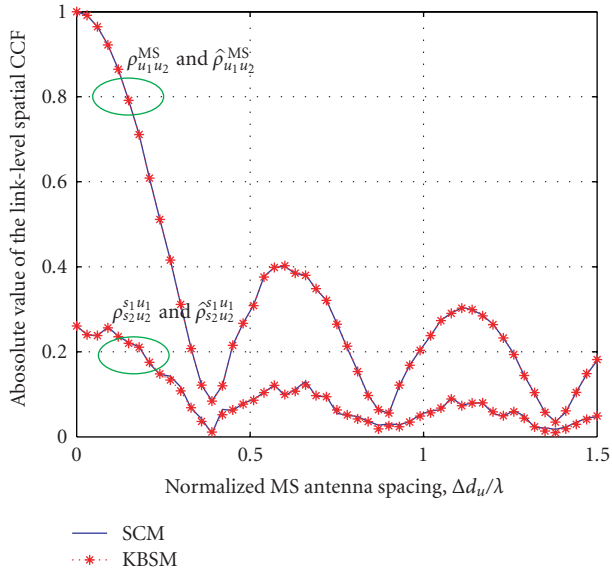

FIGURE 4: The absolute values of the link-level spatial CCFs of the SCM and KBSM with Gaussian subpath PASs ($\Delta d_s/\lambda = 1$, $\theta_{\mathrm{BS}} = 50°$, $\theta_{\mathrm{MS}} = 195°$, BS AS = 5°, MS AS = 35°).

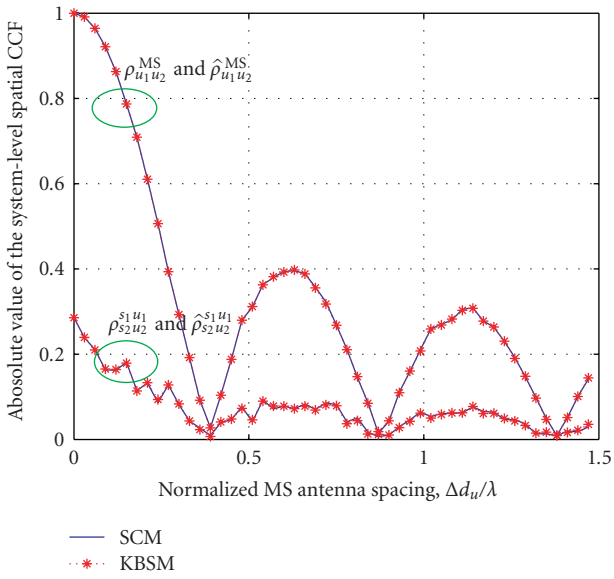

FIGURE 5: The absolute values of the system-level spatial CCFs of the SCM and KBSM with Gaussian subpath PASs ($\Delta d_s/\lambda = 1$, BS AS = 5°, MS AS = 35°).

both the SCM and KBSM. The cluster position parameters $\delta_{n,\mathrm{AoD}} = \hat{\delta}_{\mathrm{AoD}}$ and $\delta_{n,\mathrm{AoA}} = \hat{\delta}_{\mathrm{AoA}}$ are still random variables following the corresponding distributions in the link level, while both $\theta_{\mathrm{BS}} = \hat{\theta}_{\mathrm{BS}}$ and $\theta_{\mathrm{MS}} = \hat{\theta}_{\mathrm{MS}}$ are considered as random variables uniformly distributed over $[0, 2\pi)$ [14]. Again, the system-level spatial CCFs of the SCM match very closely those of the KBSM. The conclusion we can draw is that the spatial separability is also a property of the SCM at the system level.

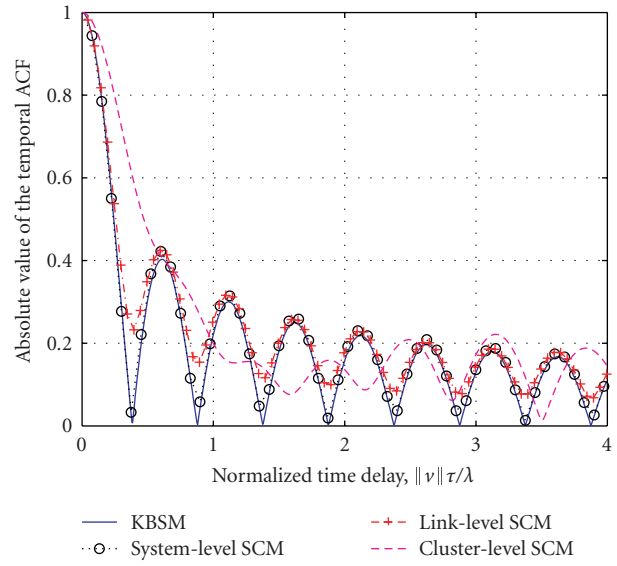

FIGURE 6: The absolute values of the temporal ACFs of the KBSM and SCM at the cluster level, link level, and system level ($\theta_v = 60°$).

To summarize, the KBSM has the property of the spatial separability at all the three levels, while the SCM exhibits the spatial separability only at the link and system levels, not at the cluster level.

4.2. *Temporal ACFs*

The temporal ACF $\hat{r}(\tau) = J_0(2\pi\|v\|\tau/\lambda)$ of the KBSM remains static at all the three levels. For the SCM, however, the expression (12) clearly shows that $r(\tau)$ varies at different levels. Figure 6 compares the absolute values of the temporal ACFs of the KBSM and SCM at the three levels. For the calculation of (12), $\theta_v = 60°$ and the rest angle parameters at different levels were taken as specified in Section 4.1. As expected, the temporal ACFs of the SCM at the cluster level or link level show substantial variations across different runs. At the system level, both models tend to have the identical ACFs. This indicates that the spatial-temporal separability is fulfilled for the SCM only at the system level, not at the cluster and link levels. In the case of the KBSM, the spatial-temporal separability is always its property at any level. Hence, the KBSM actually only models the average spatial-temporal behavior of MIMO channels, while the SCM provides us with more detailed information about variations across different realizations of MIMO channels. Clearly, a single KBSM is not sufficient for system-level simulations.

5. CONCLUSIONS

In this paper, we have proposed to compare the spatial-temporal correlation characteristics of the 3GPP SCM and KBSM at three levels. Theoretical studies clearly show that the spatial CCF of the SCM is related to the joint distribution of the AoA and AoD, while the KBSM calculates the

spatial CCF from independent AoA and AoD distributions. Under the conditions that the number of subpaths tends to infinity in the SCM, two correlated links share one antenna at either end, and the same set of angle parameters is used, the two models tend to be equivalent. Compared with uniform and Laplacian functions, it turns out that the Gaussian-shaped subpath PAS enables the KBSM to best fit the 3GPP SCM in terms of the spatial CCFs. It has also been demonstrated that the spatial separability is observed for the SCM only at the link and system levels, not at the cluster level. The spatial-temporal separability is a property of the SCM only at the system level, not at the cluster and link levels. The KBSM, however, exhibits both the spatial separability and the spatial-temporal separability at all the three levels.

Although the KBSM has the advantages of simplicity and analytical tractability, it only describes the average spatial-temporal properties of MIMO channels. On the other hand, the SCM is more complex but allows us to sufficiently simulate the variations of different MIMO channel realizations. Therefore, the SCM gives more insights of MIMO channel mechanisms. A tradeoff between model accuracy and complexity must be considered in terms of the use of the SCM and KBSM.

ACKNOWLEDGMENT

The authors appreciate the helpful comments from Dr. Dave Laurenson, University of Edinburgh, UK.

REFERENCES

[1] I. E. Talatar, "Capacity of multi-antenna Gaussian channels," Tech. Rep., AT&T Bell Labs, Florham Park, NJ, USA, June 1995.

[2] G. J. Foschini and M. J. Gans, "On limits of wireless communications in a fading environment when using multiple antennas," *Wireless Personal Communications*, vol. 6, no. 3, pp. 311–335, 1998.

[3] V. Tarokh, H. Jafarkhani, and A. R. Calderbank, "Space-time block codes from orthogonal designs," *IEEE Transactions on Information Theory*, vol. 45, no. 5, pp. 1456–1467, 1999.

[4] G. J. Foschini, "Layered space-time architecture for wireless communication in a fading environment when using multi-element antennas," *Bell Labs Technical Journal*, vol. 1, no. 2, pp. 41–59, 1996.

[5] H. Bölcskei and A. J. Paulraj, "Space-frequency coded broadband OFDM systems," in *Proceedings of the IEEE Wireless Communications and Networking Conference (WCNC '00)*, vol. 1, pp. 1–6, Chicago, Ill, USA, September 2000.

[6] D.-S. Shiu, G. J. Foschini, M. J. Gans, and J. M. Kahn, "Fading correlation and its effect on the capacity of multielement antenna systems," *IEEE Transactions on Communications*, vol. 48, no. 3, pp. 502–513, 2000.

[7] J. P. Kermoal, L. Schumacher, K. I. Pedersen, P. E. Mogensen, and F. Frederiksen, "A stochastic MIMO radio channel model with experimental validation," *IEEE Journal on Selected Areas in Communications*, vol. 20, no. 6, pp. 1211–1226, 2002.

[8] A. Abdi, J. A. Barger, and M. Kaveh, "A parametric model for the distribution of the angle of arrival and the associated correlation function and power spectrum at the mobile station," *IEEE Transactions on Vehicular Technology*, vol. 51, no. 3, pp. 425–434, 2002.

[9] L. Schumacher, L. T. Berger, and J. Ramiro-Moreno, "Recent advances in propagation characterisation and multiple antenna processing in the 3GPP framework," in *Proceedings of the 26th General Assembly of International Union of Radio Science (URSI '02)*, Maastricht, The Netherlands, August 2002.

[10] A. Abdi and M. Kaveh, "A space-time correlation model for multielement antenna systems in mobile fading channels," *IEEE Journal on Selected Areas in Communications*, vol. 20, no. 3, pp. 550–560, 2002.

[11] G. J. Byers and F. Takawira, "Spatially and temporally correlated MIMO channels: modeling and capacity analysis," *IEEE Transactions on Vehicular Technology*, vol. 53, no. 3, pp. 634–643, 2004.

[12] M. Lu, T. Lo, and J. Litva, "A physical spatio-temporal model of multipath propagation channels," in *Proceedings of the 47th IEEE Vehicular Technology Conference (VTC '97)*, vol. 2, pp. 810–814, Phoenix, Ariz, USA, May 1997.

[13] 3GPP, R1-02-0181, "MIMO discussion summary," January 2002.

[14] 3GPP, TR 25.996, "Spatial channel model for multiple input multiple output (MIMO) simulations (Rel. 6)," 2003.

[15] 3GPP, R1-050586, "Wideband SCM," 2005.

[16] L. Correia, *Wireless Flexible Personalised Communications—COST 259 Final Report*, John Wiley & Sons, New York, NY, USA, 2001.

[17] P. J. Smith and M. Shafi, "The impact of complexity in MIMO channel models," in *Proceedings of IEEE International Conference on Communications (ICC '04)*, vol. 5, pp. 2924–2928, Paris, France, June 2004.

[18] A. Giorgetti, P. J. Smith, M. Shafi, and M. Chiani, "MIMO capacity, level crossing rates and fades: the impact of spatial/temporal channel correlation," *Journal of Communications and Networks*, vol. 5, no. 2, pp. 104–115, 2003.

[19] H. Xu, D. Chizhik, H. Huang, and R. Valenzuela, "A generalized space-time multiple-input multiple-output (MIMO) channel model," *IEEE Transactions on Wireless Communications*, vol. 3, no. 3, pp. 966–975, 2004.

[20] L. Schumacher, K. I. Pedersen, and P. E. Mogensen, "From antenna spacings to theoretical capacities - guidelines for simulating MIMO systems," in *Proceedings of the 13th Annual IEEE International Symposium on Personal Indoor and Mobile Radio Communications (PIMRC '02)*, vol. 2, pp. 587–592, Lisbon, Portugal, September 2002.

[21] W. C. Y. Lee, "Effects on correlation between two mobile radio base-station antennas," *IEEE Transactions on Communications*, vol. 21, no. 11, pp. 1214–1224, 1973.

[22] F. Adachi, M. Feeny, A. Williamson, and J. Parsons, "Crosscorrelation between the envelopes of 900 MHZ signals received at a mobile radio base station site," *IEE Proceedings—Part F: Communications, Radar and Signal Processing*, vol. 133, no. 6, pp. 506–512, 1986.

[23] J. Salz and J. H. Winters, "Effect of fading correlation on adaptive arrays in digital mobile radio," *IEEE Transactions on Vehicular Technology*, vol. 43, no. 4, pp. 1049–1057, 1994.

[24] K. I. Pedersen, P. E. Mogensen, and B. H. Fleury, "Spatial channel characteristics in outdoor environments and their impact on BS antenna system performance," in *Proceedings of the 48th IEEE Vehicular Technology Conference (VTC '98)*, vol. 2, pp. 719–723, Ottawa, Canada, May 1998.

[25] W. C. Jakes, Ed., *Microwave Mobile Communications*, IEEE Press, Piscataway, NJ, USA, 1994.

[26] K. I. Pedersen, P. E. Mogensen, and B. H. Fleury, "A stochastic model of the temporal and azimuthal dispersion seen at the base station in outdoor propagation environments," *IEEE Transactions on Vehicular Technology*, vol. 49, no. 2, pp. 437–447, 2000.

[27] J. Salo, G. Del Galdo, J. Salmi, et al., "MATLAB implementation of the 3GPP Spatial Channel Model (3GPP TR 25.996)," January 2005, http://www.tkk.fi/Units/Radio/scm.